IET Image Processing

Research Article

IET Journals
The Institution of Engineering and Technology

Automatic detection of multiple sclerosis lesions using Mask R-CNN on magnetic resonance scans

ISSN 1751-9659
Received on 21st July 2020
Revised 27th October 2020
Accepted on 30th November 2020
E-First on 23rd February 2021
doi: 10.1049/iet-ipr.2020.1128
www.ietdl.org

Mehmet Süleyman Yıldırım[1], Emre Dandıl[2] ✉

[1]*Computer Technology Department of Sogut Vocational School, Bilecik Seyh Edebali University, Gulumbe Campus, Bilecik, Turkey*
[2]*Department of Computer Engineering, Bilecik Seyh Edebali University, Gulumbe Campus, Bilecik, Turkey*
✉ *E-mail: emre.dandil@bilecik.edu.tr*

Abstract: Multiple Sclerosis (MS) causes the central nervous system to malfunction due to inflammation surrounding nerve cells. Detection of MS at an early stage is very important to prevent progressive MS attacks. Clinical findings, cerebrospinal fluid examinations, the evoked potentials, magnetic resonance imaging (MRI) findings have an important role in the diagnosis and follow-up of MS. However, many of the findings on MRI may indicate brain disorders other than MS. In addition, the clinical practices accepted by physicians for MS detection are very limited. In this study, a Mask R-CNN based method in two dataset is proposed for the automatic detection of MS lesions on magnetic resonance scans.We also improved the ROI detection stage with RPN in the Mask R-CNN to easily adapt for different lesion sizes. MS lesions in different sizes in the dataset are successfully detected with 84.90% Dice similarity rate and 87.03% precision rates using the proposed method. In addition, volumetric overlap error and lesion-wise true positive rate are obtained as 12.97% and 73.75%, respectively. Moreover, performance tests of the use of different numbers of GPU hardware structures are also performed and the evaluation of its effects on processing speed is performed on experimental studies..

1 Introduction

Multiple sclerosis (MS) is a neurological disease that affects the nervous system. This disease causes inflammation by damaging myelin sheaths which surrounds and isolates nerve fibres in the central nervous system (CNS) [1]. MS affects the white and grey matter in the brain, spinal cord and optic nerve. In addition, MS is a chronic inflammatory, demyelinating and neurodegenerative CNS disease. Although the cause of MS is not known precisely, it is believed to involve a combination of genetic susceptibility, abnormalities in the immune system and environmental factors that combine to trigger disease [2].

MS is one of the most common causes of non-traumatic diseases among young and middle-aged adults. Healthcare costs directly related to MS are estimated to be more than 10 billion dollars in the USA annually [3]. Moreover, it is known that more than 2 million people worldwide have MS [4]. In a worldwide study, it is stated that the number of MS patients increased from 2.3 million in 2013 to 2.8 million in 2020 [5]. It is seen that the number of people with MS disease varies by country [6]. The rate of MS case is between 110 and 140 per 100.000 people in the northern regions of the USA, between 57 and 78 people in the southern regions, between 115 and 140 people in Western Europe and between 81 and 101 people in Australia [7]. In addition, it has been put forth by the studies that ∼20,000 people die per year due to MS disease [6].

MS is progressively divided into four types such as relapsing-remitting MS (RRMS), secondary progressive MS (SPMS), primer progressive MS and relapsing progressive MS. The frequency of MS attacks varies in each progressive and the daily life of the patient is adversely affected. Permanent disorders may also occur in the patients in the following stages. The most common type of MS is RRMS and the rate of progression of this type to SPMS in five years is over 50% [1, 8].

A physician usually follow some procedures to diagnose MS such as looking for clinical evidence of damage in at least two separate areas of the CNS, test whether the damaged areas change at least one month intervals and monitoring whether symptoms last for more than 24 h and whether they occur at different times for a month or more, investigation of MS lesion in MR images, examination of cerebrospinal fluid and oligoclonal bands [9]. In addition, there is no single diagnostic test for MS. The criteria for diagnosis include the detection of chronic inflammation of the CNS based on the evidence of at least two different lesions (such as plaque or trace) in the white matter in the brain, examining the progressive of the disease in at least two different episodes in the CNS, and detection of chronic inflammation of CNS, which is determined by the analysis of cerebrospinal fluid. The presence of one or more of these criteria allows a general diagnosis of MS, which may be updated according to the subsequent progressive of the disease [8].

The early diagnosis of MS disease can contribute to preventing MS attacks that progress along with the treatment processes to be applied. Clinical signs and symptoms, cerebrospinal fluid examinations and magnetic resonance imaging (MRI) findings are used in the diagnosis of MS disease. In particular, the widespread use of MRI has figured the diagnosis and following up of MS disease. However, many of the findings on MR images can be symptoms of brain disorders other than MS. For instance, lesions caused by migraine and some vascular disorders, brain tumours, pseudo-brain tumours may be similar to MS lesions [10]. Nowadays, various criteria are used to overcome this confusion. However, it is observed that additional methods are required to support MR findings, to facilitate diagnosis, to contribute to the determination of MS course types and to make suspicious situations more evident. Despite all these detection methods, diagnosing MS by the physician can still be very challenging. If vague neurological symptoms in young adults are accompanied by MR findings in white matter, it becomes easy to diagnose MS. In a study, it is stated that the main reason for the false diagnosis of MS is non-specific white matter abnormalities [11]. Therefore, while making a diagnosis of MS, it is required to utilise from many secondary tools and methods besides findings of MR.

MRI is of great importance in the diagnosis of MS. Detection of all brain disorders, including MS, and follow-up the change of damage on brain MR images comprise a major challenge for physicians. While it is of great importance to notice minor changes of the lesions, it is overlooked in some cases. Following the changes in MR images is considered as an important image processing issue [12–15]. The diagnosis of MS can also be similar

to be seen with other white matter diseases such as neuro-myelitis optica [16], acute cerebral infarction [17], acute diffuse encephalomyelitis [18]. Therefore, accurate diagnosis of MS disease with a non-invasive method such as MRI is very important in planning the treatment of patients.

Computer-aided detection systems based on the imaging technologies are significant in the segmentation, detection and classification of medical images [19]. The main goal in these systems is to achieve an automatic method [20]. The segmentation of medical images is the most important application and visualisation process. It provides a second tool for medical doctors to identify the disease in the body without surgery operations [21]. Such a system for detecting MS lesions on MR images reduces the time of image analysis, allows the detection phase to be automated and provides an accurate treatment plan by determining the exact boundaries of the lesions.

In this study, a state-of-art method is proposed for the automatic detection of MS using Mask regional convolutional neural network (R-CNN) on MR scans. The MS dataset used in the study has a follow-up structure and includes MR images obtained from different MR scanners at different periods. Since there are both small and large MS lesions in the datasets, it is clear to choose an region of interest (ROI) that can adapt to the whole lesion types. Thus, in our study, we improved the ROI detection stage with region proposal network (RPN) in the Mask R-CNN. In addition, this study presents a secondary tool to facilitate the decision making of physicians for detection of MS on a dataset of this scale. In the study, firstly, the labels of the lesions in the dataset, which are suitable for Mask R-CNN, are arranged and then the training process is completed and the weights are obtained. Then the obtained weights are subjected to validation process. In addition, the performance tests of the study are evaluated on the GPU and the Multi-GPU. Therefore, the hardware efficiency of the system is investigated. The rest of the paper is organised as follows. In Section 2, a survey of the related studies is presented. The material and method, the used dataset and Mask R-CNN architecture are explained in detail in Section 3. In Section 4, experimental studies and their results are evaluated and the proposed model is discussed in Section 5. In the final section, comprehensive evaluation and the result of the study are presented.

2 Related works

There are many studies in previous on issues such as the diagnosis, follow-up and change detection for lesions of MS disease. In the conducted previous studies, besides the studies that use clinical methods for the detection of MS on MR data, it is also seen that studies using many machine learning methods and using deep learning methods have become prominent in recent years.

In the field, many studies have been carried out in various topics for the detection of MS on MR images for many years [2, 22, 23]. Before the MR imaging technologies developed so much, important studies were carried out by physicians in the clinical field and MS lesions were visually detected by radiologists [9, 24, 25]. However, manual segmentation of MS lesions by experts takes a lot of time and is quite tiring. In addition, it is open to human error and each expert can draw different inferences about the case [26]. Significant developments were provided in the diagnosis of MS with the use of computer-aided systems [27, 28]. In addition, studies based on whether there are MS lesions on MR images with learning algorithms are also proposed [29]. The automatic segmentation of MS lesions can be categorised as supervised and unsupervised techniques in terms of machine learning. The unsupervised techniques are generally cluster-based approaches and formed according to the intensity features of the data. However, in cluster-based methods, the uncertainty of how to select the optimum number of clusters and features can reduce the performance in segmentation results. Although more successful segmentation results can be achieved in the supervised learning approaches, determination of the prior knowledge required for verification by an experienced radiologist can be seen as the disadvantage of the system [30]. On the other hand, in base learning approaches, since a robust training phase is required before segmentation, the performance can be low in detecting small MS lesions. In addition, in recent years, successful results were obtained in MS detection, as in many areas, in the studies using deep learning models. In these studies, high performance is obtained in datasets with low data numbers, whereas in large datasets containing different sized lesions, it is seen that the performance decreases.

Bosc *et al.* in their study, they automatically detected the change in the patient's periodic follow-up using MS lesions and healthy MR images. The framework application was prepared in the study for comparing the expert's view with the framework's results [12]. In another study, Souplet *et al.* [31] used basic image processing techniques for MS detection. They detected the brain region by normalising and focusing on three different MR sequences and highlighted the regions with MS suspicion by performing maximisation on T1 and T2 sequences via an algorithm. Schmidt *et al.*, on the other hand, developed an algorithm for automatic lesion detection using MR images to assist in the examination and decision making of MS disease. In the study, as a result of the evaluation of MS lesions of different sizes obtained by 3 T scanner with mathematical methods, a good compliance with lesions determined by manual tracking was achieved [32]. For the detection of MS lesions, Roura *et al.* developed a tool, and test procedures were carried out on patient data obtained from different scanners. In their study, firstly white matter and then lesions in this region were detected with the developed tool [33]. Zhang *et al.* [34] compared the detection of MS lesions on a dataset using nearest neighbour algorithm, support vector machines and decision tree. In another study, Wu *and* Lopez performed lesion detection in MR slices using Haar wavelet transforms, principal component analysis and logistic regression [35].

Many studies have been conducted on the MR images to detect MS lesions using different machine learning methods [36–38]. Some studies have also been in recent years proposed using deep learning techniques for MS detection. In a study that performed MS lesion detection using the convolutional neural networks (CNNs), high detection performance was not achieved [39]. Zhang *et al.* conducted a study for automatic MS detection in the fully-connected layer using dropout and parametric ReLu. Parametric rectified linear unit and dropout techniques were added to the developed CNN, and other model was developed with ten layers (seven layers of convolution layer and three fully-connected layer) deep neural network [40]. In another study, Maleki *et al.* proposed to increase the performance of MS detection by simultaneously on T1-w and FLAIR images of the same patient using CNN [41]. Wang *et al.* detected MS lesions using 14-layer CNN model combined with batch normalisation, dropout and stochastic pooling techniques [42]. Ravnik *et al.* conducted a study on automatic detection of MS data using CNN. In their study, firstly CNN training was completed using making pre-processes such as histogram-based standardisation, normalisation on MR images and rotating them according to axes. Then, tests were done by adding the images obtained from the same or different MR scanners to the dataset [38]. Nair *et al.* developed a model for the detection of MS lesions using 3D CNN. In their study, they emphasised that the dropout layer is important in determining the lesions. They also suggested that the high rate of false detection of small lesions positively affected the detection of other sizes [43]. Birenbaum and Greenspan conducted a study on the detection of MS lesions using the multi-view L-CNN model. They argued that the proposed method is more successful than CNN models for detection of MS lesions. Since dataset of five patients was used in the study, its scope seems to be limited [44]. Atlason *et al.* provided MS lesion detection on two different databases with the CNN auto-encoder named SegAE [45].

Although it is difficult to compare previous studies on the detection of MS disease by using computer-assisted methods, due to reasons such as not using the same dataset, different detection methods and various similarity criteria, general evaluation of some studies proposed for the detection of MS is presented in Table 1.

Table 1 Previous studies in MS detection and evaluations of these studies

Reference	Database	Number of subject	MRI sequences	Methodology	Evaluations/limitations
Bosc *et al.* [12]	their own dataset	8	T1-w, FLAIR, multimodal RARE	automatic change detection using a non-linear intensity normalisation method	the results of the study were not measured by general metrics. Not tested with a sufficient amount of dataset
Souplet *et al.* [31]	MICCAI 2008	45	T1-w, T2-w, T2-w FLAIR	automatic segmentation MS lesions based on image pre-processing, morphological operations and expectation and maximisation algorithm	high performance was not achieved
Schmidt *et al.* [32]	their own dataset	70	T2-w FLAIR, 3D T1-w	an automated tool for MS lesion detection using the developed a segmentation algorithm	high performance was not achieved and it was not implemented on different datasets
Maleki *et al.* [41]	their own dataset	150	not available *(NA)*	classification of MS lesion via CNN	evaluations were limited to lesion detection only
Roura *et al.* [33]	MICCAI 2008, their own dataset (2)	70 + 45 + 14	T1-w, T2-w, FLAIR	MS lesion segmentation via an automated toolbox based on image processing techniques	requires pre-processing
Brosch *et al.* [36]	MS lesion segmentation challenge 2008	500	T1-w, T2-w, FLAIR	segmentation of MS lesions using deep convolutional encoder networks	detection performance can be increased
Zhang *et al.* [34]	eHealth	38	T2-w	MS lesion detection using machine learning methods such as k-nearest neighbours, decision tree, support vector machine and comparison results	high accuracy performance was not achieved and it was not implemented on different datasets
Brosch *et al.* [46]	MICCAI 2008 and ISBI 2015	43 + 21 + 377	T1-w, T2-w, FLAIR	MS lesion segmentation via deep 3D convolutional encoder networks with shortcuts for multiscale feature integration	the performance rate is low compared to other studies and detection performance can be increased
Wu *and* Lopez [35]	their own dataset	67	*NA*	MS slice identification using Haar wavelet transform, principal component analysis and logistic regression	the dataset is inadequate
Birenbaum *and* Greenspan [44]	ISBI 2015	5	T1-w, T2-w, FLAIR	MS lesion segmentation using multi-view longitudinal CNN	dataset is limited to only 5 patients
Valverde *et al.* (2017) [37]	MICCAI 2008	45	T1-w, T2-w, FLAIR	a novel automated MS lesion segmentation with a cascaded 3D CNN	the structure of the model is available to develop
Zhang *et al.* [40]	eHealth, their own dataset (private)	38 + 26	T2-w	MS lesion identification using an improved CNN based on parametric ReLU and dropout	evaluations were limited to lesion detection only
Wang *et al.* [42]	eHealth, private (Zhang *et al.* [40])	38 + 26	T2-w	identification of MS lesions using 14-layer CNN with batch normalisation, dropout, and stochastic pooling	the results of the study were not measured by metrics
Ravnik *et al.* [38]	UMCL	60	T1-w, T2-w, FLAIR	lesion segmentation via CNN based different image pre-processing and augmentation methods	detection performance can be increased
Valcarcel *et al.* [47]	their own dataset	98	T1-w, T2-w, FLAIR	an automated method for segmentation of MS lesions	detection performance can be increased
Zhao *et al.* [10]	MICCAI 2008	45	T1-w, T2-w, FLAIR	MS lesion segmentation using a level set method	other databases can also be evaluated.
Atlason *et al.* [45]	the AGES-Reykjavik, MICCAI 2017	60 + 60	3D T1-w, proton density-weighted (PD-w), 2D/3D FLAIR	lesion segmentation using a supervised CNN autoencoder	the structure of the model is available to develop
Gabr *et al.* [48]	their own dataset	1008	3D T1-w, T2-w, PD-w, 2D FLAIR	lesion segmentation in MS using fully convolutional neural network	the results can be compared with different methods
Nair *et al.* [43]	their own dataset	1064	T1-w, T2-w, FLAIR, PD-w	detection and segmentation of 3D MS lesions via CNN based on Monte Carlo dropout	detection performance can be increased
Gessert *et al.* [49]	their own dataset	89 + 33	FLAIR	MS lesion segmentation with attention-guided two-path CNNs	the results can be compared with different methods
Wang *et al.* [30]	MICCAI 2008	45	T1-w, T2-w, FLAIR	MS lesion segmentation in brain MRI using an adaptive sparse Bayesian model combined with probabilistic label fusion	detection performance can be increased

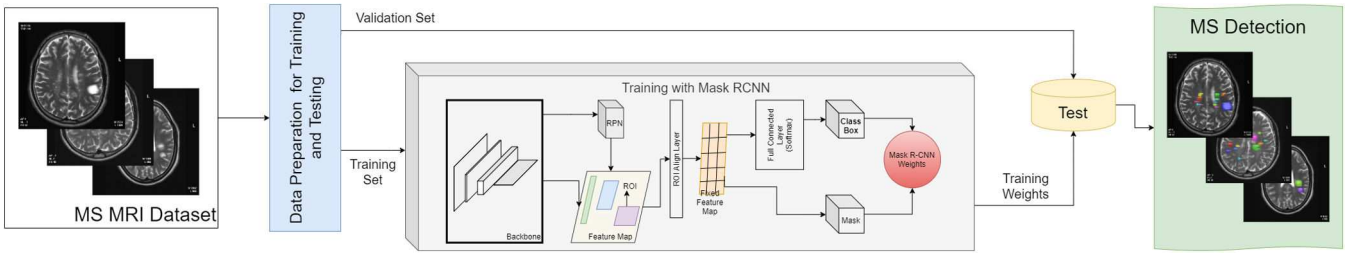

Fig. 1 *General block diagram of the methodology of the proposed system for MRS detection using Mask R-CNN on MR images*

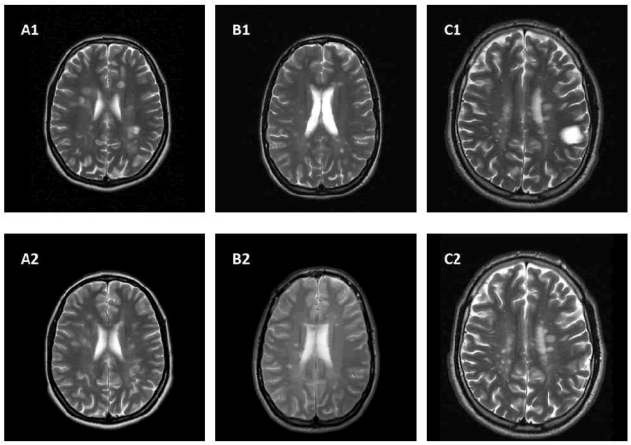

Fig. 2 *Sample MR images from the MS database of the eHealth lab. A1, B1 and C1 MR slices were obtained from the patient's first scan. A2, B2 and C2 show the MR image of the near point taken from the 6 or 12 month periodic examination of the same patients*

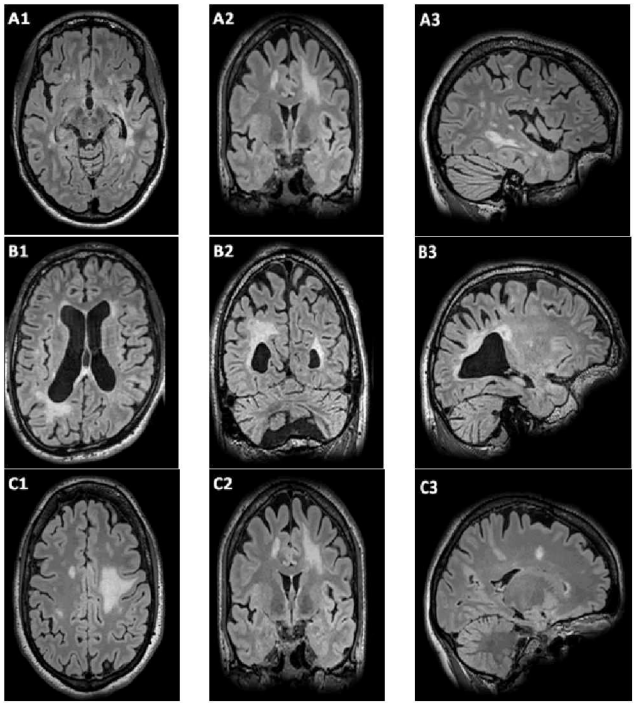

Fig. 3 *Some MRI scans with MS lesions in the UMCL MS dataset. A1, B1, C1 show the scanning in the axial plane of the MR images, A2, B2, C2 coronal plane and A3, B3, C3 in the sagittal plane*

3 Proposed method

In this study, a Mask R-CNN based approach was proposed for the detection of MS lesions on two public MS datasets. In the study, firstly data preparation processes were carried out on the dataset. The training phase was carried out using the GPU hardware structure with Mask R-CNN on the prepared dataset. After the training phase was completed, the test performance of system was performed on the dataset for MS lesion detection. The methodology of the proposed system is shown in detail in Fig. 1.

3.1 MS datasets

We evaluated our Mask R-CNN based method on two public datasets such as MS dataset of eHealth laboratory and UMCL MS dataset for MS lesion detection. In this way, these dataset provide comparison our results with many state-of-the-art methods.

MS dataset of eHealth laboratory: One of the datasets used in this study for the detection of MS on MR images was provided by the University of Cyprus eHealth Laboratory for scientific studies [50]. The dataset (eHealth) includes both the images of the patients for first examination and the images obtained during their 6–12 months periodic examinations. The MR images in the dataset were acquired using a T2-w sequence. The lesions on each MR slices were marked by specialist doctors. MR images of some patients with MS lesions taken from the eHealth MS dataset are denoted in Fig. 2. The dataset used in the study has a total of 1838 MR images collected from 38 patients. Above 677 of these images have 1777 MS lesions, and the boundaries of the lesions on MR images were labelled by experts. Loizou *et al.*, that provided the dataset, conducted studies on multi-scale amplitude modulation frequency modulation, white matter classification, image normalisation and quantitative tissue analysis of white matter lesions (WMH) in brain MR images of this dataset [51–54]. In addition, in some studies that detected MS lesions using CNN on this dataset, only images with and without MS lesions were classified [34, 40]. The dataset used contains an average of 22 slices per patient. In each scan, MR slices were obtained at the axial plane at 5 mm thickness. Due to the thickness of the slices, the lesions in successive images are not in the form of continuation of each other, but in different patterns. For this reason, randomly selected images in the training and test sets do not overlap each other as lesion patterns even if they are from the same patient. In addition, since there are often many MS lesions in an MR section, the total number of lesions in the dataset is high. However, in the training and test sets in our study, it was ensured that there was a homogeneous distribution for all patients, rather than many MR slices of the same patient.

UMCL MS dataset: Another MS dataset used in this study, 3D MR image database of MS patients with WMH segmentations of University Medical Center Ljubljana (UMCL) contains MR images of MS patients with consensus by ground truth segmentations of WMHs [55, 56]. In this public dataset, a total of 30 MS patients were scanned using a 3 T Siemens Magnetom Trio MR system. MR scan of each patient consisted of 2D T1-w, 2D T2-weighted (T2-w) and 3D FLAIR images. The acquisition parameter values of MR scans were issued by Lesjak *et al.* [55]. In the database, the UMCL approved the use of MRI data for all 30 subjects. In this study, we used the 2D MR scans and their ground truths in axial plane of the space of FLAIR image for lesion segmentation since the segmentation procedures in the dataset mainly performed on the axial cross-sections. Fig. 3 shows some MRI scans with MS lesions in the UMCL MS dataset.

3.2 Mask R-CNN

CNN architecture, which is the common infrastructure of deep learning models, is generally based on a structure that classifies the data with a fully connected layer after converting the data into a plane with procedures such as convolution and padding [57]. Basic

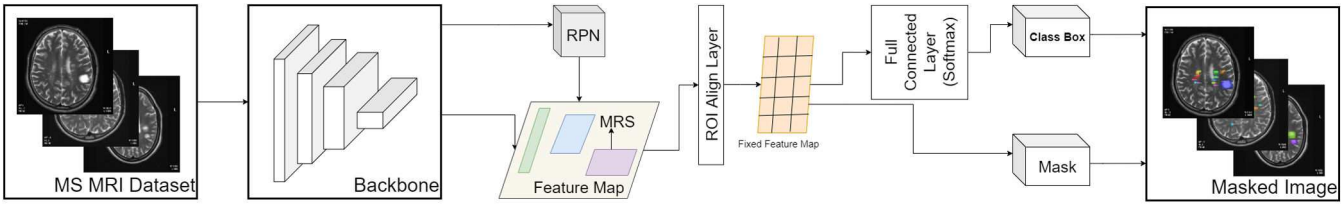

Fig. 4 *General block overview of Mask R-CNN architecture used in this study*

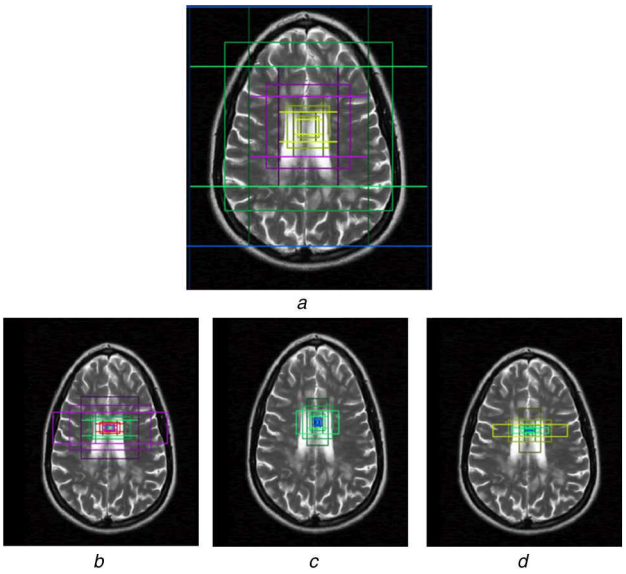

Fig. 5 *Improved ROI detection stage with RPN*
(a) Original ROI generated by Mask R-CNN, ***(b)***, ***(c)***, ***(d)*** Improved ROI generation with dynamic threshold

architecture of the concept of deep learning is accepted as CNN. This architecture consists of input layer, convolution layer, padding, ReLu layer, pooling layer, fully-connected layer, dropout layer and classification layer [57, 58]. Another CNN infrastructure, R-CNN, is an object recognition algorithm that segments data by identifying bounding boxes where objects are likely to be found and runs the detection algorithm to find possible objects inside the boxes [59]. In many studies, regions were determined using R-CNN and it has always been desired to find faster and more accurate results. Mask R-CNN has been developed by adding masking feature to faster R-CNN on the idea that a mask can be applied to detect pixel-based region on the image and then a faster and more precise result can be obtained [60, 61].

Mask R-CNN architecture, which is an extension of Faster R-CNN, is a very important deep learning model that can be used to select targets on images. The block diagram of the Mask R-CNN architecture proposed in this study is shown in Fig. 4. As with Faster R-CNN, Mask R-CNN model basically has a structure consisting of two main stages [62]. In the first stage, all possible regions are determined for the object detection, as known RPN. This stage is passed through the determined backbone such as ResNet50 and ResNet101. In these backbone structures, a spatial order is created on the input data to extract features and create feature map. As a result of the created feature map, class of the object in the ROI is determined via RPN. In the second stage, the proposals are classified and mask and bounding box are predicted simultaneously. However, Mask R-CNN generates a binary mask related label and bounding box for each ROI [60]. As a result, many irrelevant ROIs can be generated that reduce the classification accuracy. Since classification in Mask R-CNN is closely related to the generated masks, ROIs need to be estimated accurately and appropriately. As there are very small or very large MS lesions in the datasets used in our study, it is obvious to choose an ROI that can adapt to both lesion types. Therefore, in our study, we improved the ROI detection stage with RPN in the Mask R-CNN to easily adapt to changing lesion sizes. Number of ROIs is selected using a dynamic threshold value with non-maximum suppression after comparing ROI and ground truth. In the improved ROI detection approach, small MS lesions were mainly largely detected using Mask R-CNN to a large extent. In the standard case, while the accuracy performance was low in the detection of lesions smaller than 16×16 pixels using the Mask R-CNN, the detection of lesions up to 4×4 pixels was successfully achieved thanks to the use of the improved ROI selection. In addition, while the standard ROI detection in Mask R-CNN can be provided in 32, 64, 128, 256 and 512 pixel sizes, ROI detection up to 4, 8, 16 pixels were achieved thanks to the use of the improved ROI detection in Mask R-CNN. The improved ROI detection stage with RPN is shown in Fig. 5. Afterwards, the feature map and the determined ROIs are carried to ROI-Align layer. For the classification and segmentation process in Mask R-CNN, significant regions are determined with the ROI-Align layer. On the input data, the regional areas to be segmented are determined by ROI-Align layer. ROI-Align operation, which is an important region detection structure proposed with Mask R-CNN, gives faster results since it does not make the heavy cost calculations for the regions individually, unlike ROI-Pooling. The costs of the regions determined in the ROI-Align operation are determined by the average or maximum pooling process, thus processing speed and detection performance increases [60]. Finally, a spatial order is created and the data is separated into two flows. One of them is presented to the fully-connected layer for classification and one enters full convolution network for segmentation. Thus, in this layer, classification and segmentation processes in the regions are carried out.

Various backbone structures are used in the mask R-CNN structure. These backbone structures are used primarily for feature extraction and then for segmentation of objects in specified boxes. In this study, ResNet50 and ResNet101 are structures used for the backbone structure of Mask R-CNN. In these backbone structures, the naming is referred according to the layer depth in this study. Therefore, the 50-layer ResNet structure is named as ResNet50, and the 101-layer ResNet structure is called as ResNet101. ResNet, which has a different structure from the previous models, where the network model begins to really deepen, is formed by adding residual values of the blocks that feed the next layers to the model.

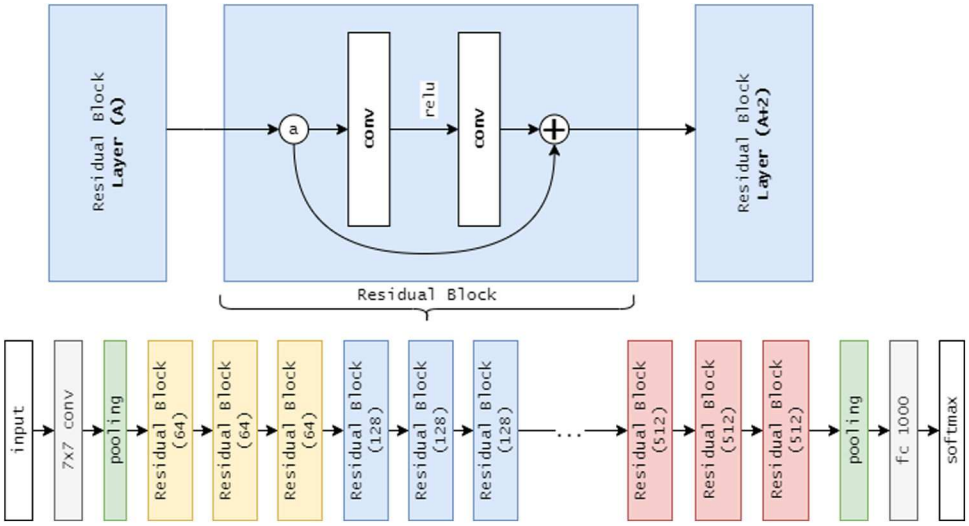

Fig. 6 *General scheme of ResNet architecture consisting of blocks*

Table 2 Configuration details of the computer used for experimental studies in this study

Hardware component	Configuration
computer	Workstation
central processor unit (CPU)	Intel Core i9–9900 K @ 5 GHz (8 Core/16 Thread)
memory (RAM)	32 GB (DDR4 2666 MHz)
mainboard	ASUS WS Z390 PRO
GPU (*x*2)	NVIDIA GeForce RTX 2080Ti 11 GB GDDR6
hard disk driver	256 GB SSD HDD + 3 TB SATA 6 Gb 3.5″ HDD

Thanks to this feature, ResNet differs from classic models. Between Linear and ReLu layers, an added value on two layers changes the calculations in the architecture. As can be seen in the ResNet architecture in Fig. 6, the value that previously came to Layer A is considered in Layer A + 2 or Layer A + 3 in some models of ResNet.

4 Experimental studies

In this study, many experimental studies were conducted to confirm the performance of the Mask R-CNN based model proposed for the detection of MS lesions on MR images, and the results and the findings were analysed. All applications performed on the proposed model in Linux environment with Python programming. For these analyses, a computer with a workstation was used and its specifications were presented in Table 2. In the study, various performance tests were performed with double GPU. The used model was developed by modifying the matterport-maskrcnn [63] which is the open source Mask R-CNN framework. Matterport-maskrcnn application was prepared for the Mask RCNN architecture [60] in Python using Keras architecture on TensorFlow framework. This application also provides GPU support and includes the structures of ResNet50 and ResNet101 backbones running on Mask R-CNN. Moreover, it allows ROI sorting and filtering, ROI visualisation, masking of different ratios, examination of weight histograms, examination of training performance on tensorboard, various measurements and visualisations on the image. Matterport-maskrcnn uses mask annotations prepared in the COCO format. Therefore, the labels of the datasets used in this study were rearranged in the json structure in COCO format.

In this study, two public MS datasets such as eHealth and UMCL were used for detection and segmentation of MS lesions. The ones with more apparent labels of MR images were selected. In the eHealth Laboratory database, 84.53% (470) of the images containing MS lesions obtained from the periodic scans of the patients were used during the training phase, and the remaining 15.47% (86) were used for the test phase. In UMCL dataset, we used 502 (83.67%) training and 98 (16.33%) test MR images for experimental studies. MS lesion labels are presented with the dataset in *.plq* format. However, since this format is incompatible with the system used in the study, it was converted to *.json* format in Matlab environment. Files in *.plq* format are read one by one and converted to *.json* format in VGG 1.6 structure. As a result of the conversion process, labels in the appropriate format for Mask R-CNN and U-Net used in our study were obtained. Afterwards, the masks were examined one by one according to their confirmations provided by experts.

The specific settings determined for the modified Mask R-CNN architecture in the proposed model in this study are given in Table 3. While determining these settings, various stages were followed and the most efficient values for model were created. For the tests conducted with double GPU, the most appropriate iteration number was specified to be as 1000 and the number of epoch was determined to be as 50, which was confirmed by the success of the tests. In our study, performance improvements were provided for the developed model on the open source framework and various improvements were made for the training phase. With the improvements during the training phase, a mini-mask size was arranged for the detection of small-sized MS lesions. In addition, class arrangements were specified according to different MS lesions sizes.

In the testing phase of the proposed model, a structure was prepared that separately calculates the weights obtained in each epoch of the training process in order to perform the performance measurements appropriately. The test performance of the system was measured by performing the process repeatedly using the weights obtained for each epoch. Mask R-CNN model proposed in the study was rearranged on two different backbones. In the study, MC-R50 was used for the model with the backbone structure ResNet50, and MC-R101 for the model with the backbone structure ResNet101. For the Mask R-CNN model proposed in the study, a training phase was carried out on ResNet50 and ResNet101 pre-trained networks with 50 and 100 epoch and 1000 iterations with single and double GPUs. Performance measurements were performed on the test set by using the weights obtained as a result of the training with the Mask R-CNN model.

In the study, dice coefficient (DC), value of overlap error (VOE), precision (PR), recall (RC) and lesion-wise true positive rate (LTPR) performance metrics were used to measure results in

Table 3 Specific settings for the application of Mask R-CNN model for experimental studies

Feature	Value	Explanations
BACKBONE	ResNet50 / ResNet101	pre-trained network model to be used
GPU_COUNT	2	GPU value at which the network will run
IMAGE_MIN_DIM	256	minimum dimensions of images in the dataset
IMAGE_MAX_DIM	512	maximum dimensions of images in the dataset
TRAIN_ROIS_PER_IMAGE	200	number of estimated regions to be found for each image during the training phase
MAX_GT_INSTANCES	100	maximum number of lesions in an image
IMAGES_PER_GPU	2	images per GPU
NUM_CLASSES	1 + 1	number of classes on lesions (MS lesion + background)
STEPS_PER_EPOCH	1000	number of step in each epoch
EPOCH_COUNT	50	number of epoch
THRESHOLD	0.5	the maximum error rate determined for the detection success of a lesion

Table 4 Structure of confusion matrix used in calculating performance metrics

		Expert decision	
	Lesion	1	0
the masked area	1 (lesion)	TP	FN
	0 (background)	FP	TN

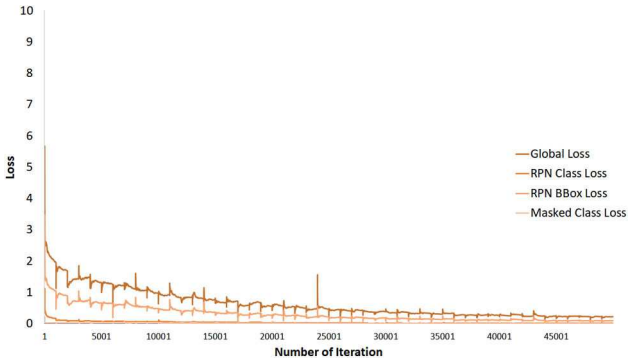

Fig. 7 *Error change graphs in the training process with MC-R50*

the experimental studies conducted for the Mask R-CNN model proposed for the detection of MS lesions. The best results in all iterations were calculated and tested for these performance measurement metrics. DC, VOE, PR and RC criteria were determined according to the true positive (TP), false positive (FP), true negative (TN) and false negative (FN) values shown in the confusion matrix in Table 4.

DC, which is shown in (1), is a criterion calculated according to the overlap amount of the region placed on the pre-selected regions. DC is a measure of compliance, and it appears that as DC's value grows, its detection performance also increases. The VOE metric, denoted in (2), shows the error rate between the expert opinion and the masked region. PR in (3), which shows how successful segmentation is in an image, refers to the ratio of correctly masked lesions to all masked lesions on the image. RC in (4), which shows how much of the lesions in an image are segmented correctly, refers to the ratio of successfully masked lesions on the image to all lesions on the image [64]. LTPR, in (5), is the number of lesions that overlap in segmentation and ground truth map divided by the total number of lesions in the ground truth map [49]. Here, LTP shows the number of lesions in the reference segmentation that overlap with a lesion in the output segmentation, and RL is the total number of lesions in the reference segmentation [65]. Low and high segmentation results are tracked with the PR given in (3) and the RC presented in (4). In these equations for metrics, the expert opinion area was named A_{ref}, and the area masked as a result of the proposed model was specified A_{mask}

$$\text{DC} = \frac{2\text{TP}}{2\text{TP} + \text{FP} + \text{FN}} = \frac{2|A_{\text{ref}} \cap A_{\text{mask}}|}{|A_{\text{ref}}| \cup |A_{\text{mask}}|} \tag{1}$$

$$\text{VOE} = \frac{\text{FN} + \text{FP}}{\text{TP} + \text{FN} + \text{FP}} = 100 \times \left(1 - \frac{|A_{\text{ref}} \cap A_{\text{mask}}|}{|A_{\text{ref}} \cup A_{\text{mask}}|}\right) \tag{2}$$

$$\text{PR} = \frac{\text{TP}}{\text{TP} + \text{FP}} \tag{3}$$

$$\text{RC} = \frac{\text{TP}}{\text{TP} + \text{FN}} \tag{4}$$

$$\text{LTPR} = \frac{\text{LTP}}{\text{RL}} \tag{5}$$

In the study, the proposed model was trained on dataset using MC-R50 and MC-R101. The training process conducted in the MC-R50 is presented in detail with the graphics in Fig. 7. The global loss shows the decrease of the general error in the training process, and masked class loss denotes the decrease in the errors of the masked classes on the training set. On the other hand, RPN class loss shows the decrease in the determination of the regions where the objects are located, and RPN Bbox loss denotes the decrease in the boundaries of the important regions.

In the proposed study, the conducted procedures for automatic detection of MS lesions on MR images with Mask R-CNN are shown step by step in Fig. 8. In the first stage, after feature extraction is conducted on the input image, ROI alignment is performed and possible important regions are determined. In the second stage, positive regions are selected among the regions. In the third stage, the boundaries of the regions that have MS lesions searched for detection are specified. In the fourth stage, the boundaries of the region are determined and the lesion detection process is completed.

The performance of the system was tested by using the weights obtained as a result of the training process with the proposed Mask R-CNN based models on the test set. The results of the DC, PR and RC metrics performed on the MC-R50 and MC-R101 for 50 epochs are denoted in Figs. 9 and 10, respectively. It is seen from these graphs that the DC value increases in the whole training process. PR values reached high values due to the successful detection of most of the lesions in the first epoch. However, the low DC value in the same epochs indicates that there are lesions in many non-lesions regions in these epochs.

The change of VOE value for MC-R50 and MC-R101 are shown for 50 epochs in Fig. 11. This figure shows the decrease in error between regions identified by the proposed model and marked by the expert. It is seen that the epochs with the VOE values reaching the minimum levels are the epochs with the highest DC performance.

In the tests performed, the values of the VOE, DC, PR, LTPR and RC metrics in the most successful epochs are shown in Table 5. As can be seen from this table, the proposed model achieved success for all metrics in the epochs where the DC criterion reached the highest level. Although it is run on the same computer under the same conditions, it is seen that MC-R101 is more successful than MC-R50 for all metrics.

In the measurement of the test performances of the proposed study, the best epoch results obtained using both models for the successfully detected lesions are shown in Table 6. In the proposed MC-R50 model, the most successful DC performance was in epoch

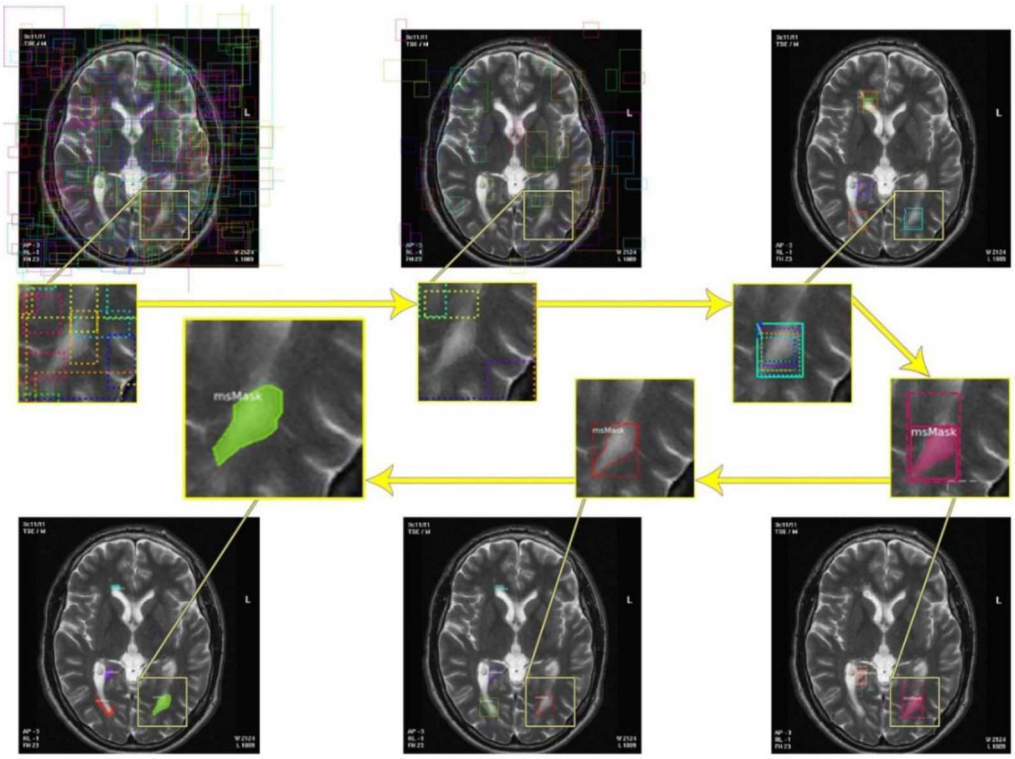

Fig. 8 *Step-by-step process for automatic detection of MS lesions using the proposed method*

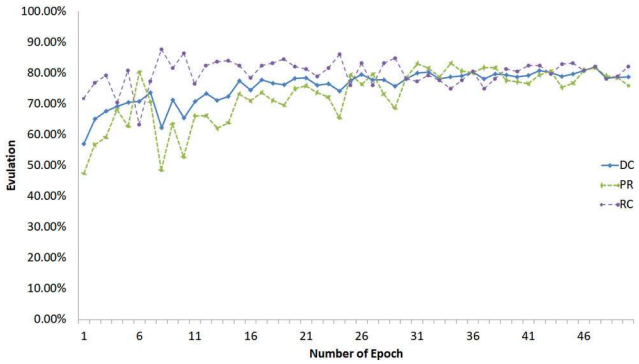

Fig. 9 *Change of performance graphs for DC, PR and RC metrics in tests with MC-R50 backbone model*

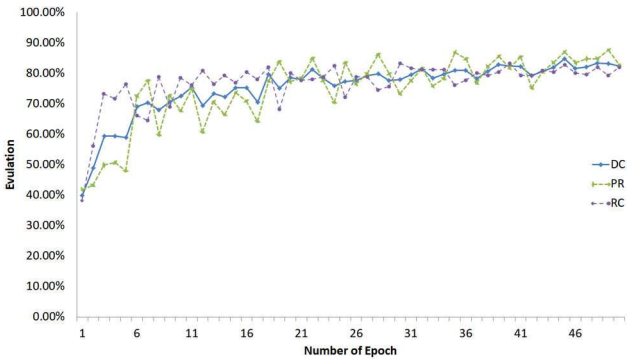

Fig. 10 *Change of performance graphs for DC, PR and RC metrics in tests with MC-R101 backbone model*

47, whereas the most successful results were obtained in epoch 44 in the MC-R101 model. As can be seen from the table, 206 of the total 251 lesions in the test set were detected with MC-R50, and 208 lesions were successfully detected with MC-R101.

The evaluation results of ten images taken from the tests performed with the best epoch weights obtained in the experimental studies carried out with the MC-R50 model are presented in Table 7. The results of the number of MS lesion (NoL), the number of the detected lesions successfully (NoDL), DC, PR, RC and VOE metrics on the selected MR images are shown in this table. It is seen that many lesions were successfully detected with the MC-R50 model. The evaluation results of ten images taken from the experimental studies carried out with the MC-R101 model are shown in Table 8. It is clearly seen in the table that the MC-R101 is more successful than the MC-R50 for detection of MS lesions. In addition, it can be concluded that the MC-R101 model is more successful in images with more lesions.

Various performance speed tests were carried out using the GPU hardware structures on the proposed model within the scope of the study. Each iteration was conducted for 73 ms on the

workstation with double GPU for the ResNet50 pre-trained network. Effect of change in GPU count (GC), steps per epoch (SPE), images per GPU (IPG) and batch size (BS) parameters of mask R-CNN on the step speed and time for an image (TI) is presented in detail in Table 9. BS value in the table is calculated as a result of $BS = GC * IPE$ equation. TI value is measured by the $TI = Step / BS$ equation. As a result of these experimental studies, it has been understood that increasing the number of GPUs and steps used in the process of processing an image has a significant contribution. These experiments were carried out with a limited dataset on the model for the solution of a difficult problem. The difficulty of the problem is thought to affect the accuracy of the time measurements. In addition, the Mask R-CNN model proposed in the tests performed on the computer with the given configurations could not be run on the CPU.

5 Discussion

Examples of MS lesions detected successfully in the experimental studies conducted on the MR images with the Mask R-CNN models proposed in this study are shown in Fig. 12. Since the lesions in the images are small, larger versions of these lesions are

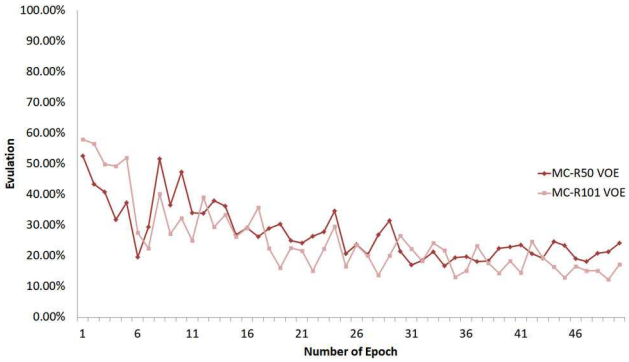

Fig. 11 *VOE change graph in tests with MC-R50 and MC-R101 backbone models*

Table 5 Performance measurement results of the proposed Mask R-CNN based model in tests

Backbone	DC, %	PR, %	RC, %	VOE, %	LTPR, %
MC-R50 FPN	81.91 ±9.89	81.75 ±8.65	82.07 ±6.12	18.25 ±4.24	69.36 ±5.79
MC-R101 FPN	84.90 ±8.97	87.03 ±8.04	82.87 ±6.78	12.97 ±2.96	73.75 ±4.94

Table 6 Comparison of the number of lesions successfully detected on the test set using each model in the proposed study

Mask R-CNN backbone	Number of lesion	Number of the detected lesions	Number of lesions detected incorrectly	Number of lesions not detected
MC-R50 FPN	251	206	46	45
MC-R101 FPN	251	208	31	43

Table 7 Results of performance metrics for ten images from the best epoch for the MC-R50

Image ID	NoL	NoDL	DC	PR	RC	VOE
AA_first_IM_00039	4	4	1.00	1.00	1.00	0.00
AA_second_IM_00236	4	4	0.89	0.80	1.00	0.20
GPE_first_IM_00038	5	4	0.89	1.00	0.80	0.20
HC_first_IM_00120	4	4	1.00	1.00	1.00	0.00
HC_second_IM_00038.	5	4	0.89	1.00	0.80	0.20
IPH_second_IM_00038	4	4	0.89	0.80	1.00	0.20
MJ_first_IM_00088.	9	8	0.94	1.00	0.89	0.11
PRI_second_IM_00018	7	7	0.93	0.88	1.00	0.13
SKS_first_IM_00016	5	4	0.89	1.00	0.80	0.20
TZN_second_IM_00016	5	5	0.91	0.83	1.00	0.17

Table 8 Results of performance metrics for ten images from the best epoch for the MC-R101

Image ID	NoL	NoDL	DC	PR	RC	VOE
AA_first_IM_00039	4	4	1.00	1.00	1.00	0.00
AA_second_IM_00236	4	4	1.00	1.00	1.00	0.00
FI_second_img013	5	5	1.00	1.00	1.00	0.00
FI_second_img016	9	7	0.88	1.00	0.78	0.22
HC_second_IM_00038	5	5	0.91	0.83	1.00	0.17
MJ_first_IM_00089	7	7	1.00	1.00	1.00	0.00
PRI_first_IM_00017	11	11	1.00	1.00	1.00	0.00
SKS_second_IM_00016	6	5	0.91	1.00	0.83	0.17
TZN_second_IM_00014	5	5	1.00	1.00	1.00	0.00
TZN_second_IM_00016	5	5	1.00	1.00	1.00	0.00

shown by connecting them below the images. In addition, the lesion coverage of the mask is shown alongside the lesions in the images. As this ratio approaches 1.0, it can be said that the detected mask and the volumetric area of the lesion overlaps successfully.

As a result of the tests, the similarities of some MS lesions evaluated as successful according to the overlap rate with the lesions determined by the experts who prepared the dataset of MR images are shown in Fig. 13. The area indicated with the red line shows the masked lesion by the proposed model, and the area shown with the green line shows MS lesions determined by the experts. In addition, it is clearly noticeable that the proposed model for some MS lesions detected better than the expert. The first of the numbers appearing on the marked lesions shown in Fig. 11 shows how much of the selected area is the lesion, and the second shows how much of the lesion is included in the selected area. Since MS lesions were very small in the study, when 50% of a lesion was detected, that lesion was evaluated as positive.

In the study, it was not possible to detect some MS lesions successfully due to reasons such as the size of the lesions in the dataset, the quality of the MR image and the differences of the scanning parameters. Some examples of lesions that could not be detected successfully are given in Fig. 14. The lesions marked with a blue box represent lesions that are either not fully detected or not detected at all. On the other hand, the lesions marked with yellow boxes represent lesions identified as positive. As can be seen, some MS lesions, although not many, were not detected using the proposed models.

We also compared the obtained detection results using Mask R-CNN with the results using U-Net, another popular segmentation algorithm, for detection MS lesions in the dataset in this study. In the U-Net architecture, there are contraction and expansion paths at both sides of the network, right and left [66, 67]. Therefore, the encoder and decoder achieve feature extraction and resolution recovery procedures [68]. In Fig. 15, visual comparisons for

Table 9 Comparison of step times in different parameters of experimental studies with single and double GPU hardware

Backbone	GC	IPG	SPE	BS	Step, ms	TI, ms
MC-R50	1	1	100	1	250	250
	1	1	1000	1	140	140
	1	2	100	2	382	382
	1	2	1000	2	223	111.5
	2	1	100	2	129	64.5
	2	1	1000	2	73	36.5
	2	2	100	4	186	46.5
	2	2	1000	4	120	30
MC-R101	1	1	100	1	263	263
	1	1	1000	1	149	149
	1	2	100	2	398	199
	1	2	1000	2	232	116
	2	1	100	2	135	67.5
	2	1	1000	2	78	39
	2	2	100	4	190	47.5
	2	2	1000	4	124	31

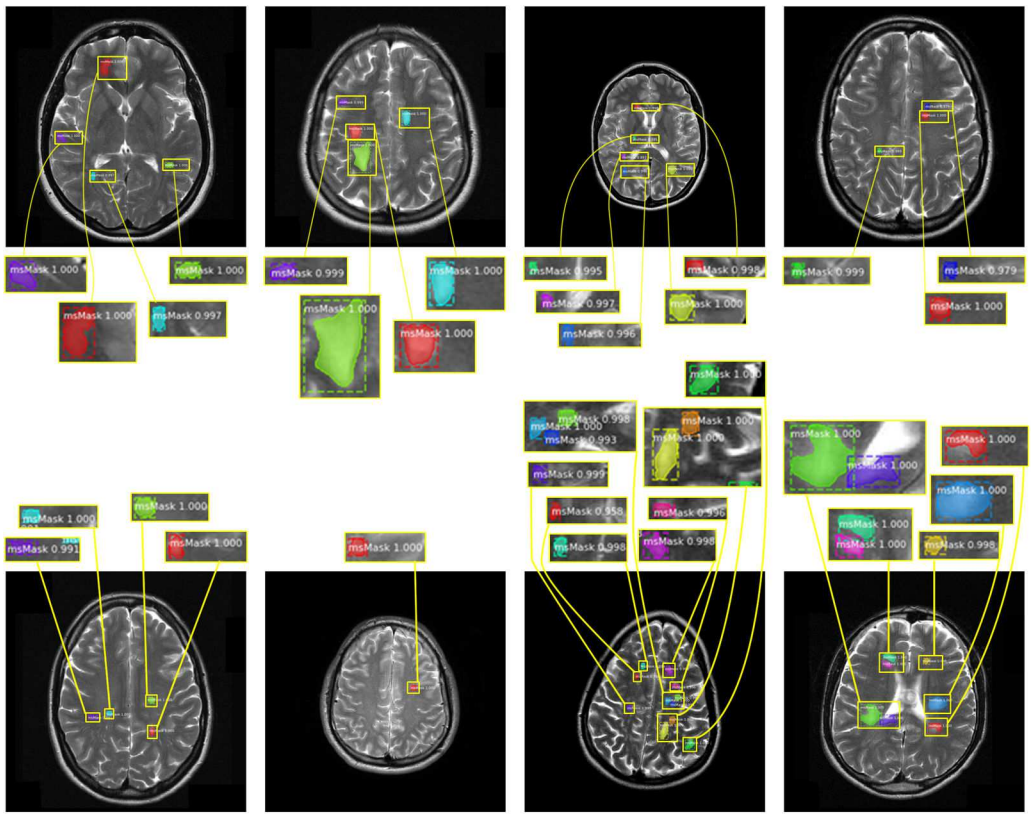

Fig. 12 *MS lesion samples successfully detected with the proposed model on MR images*

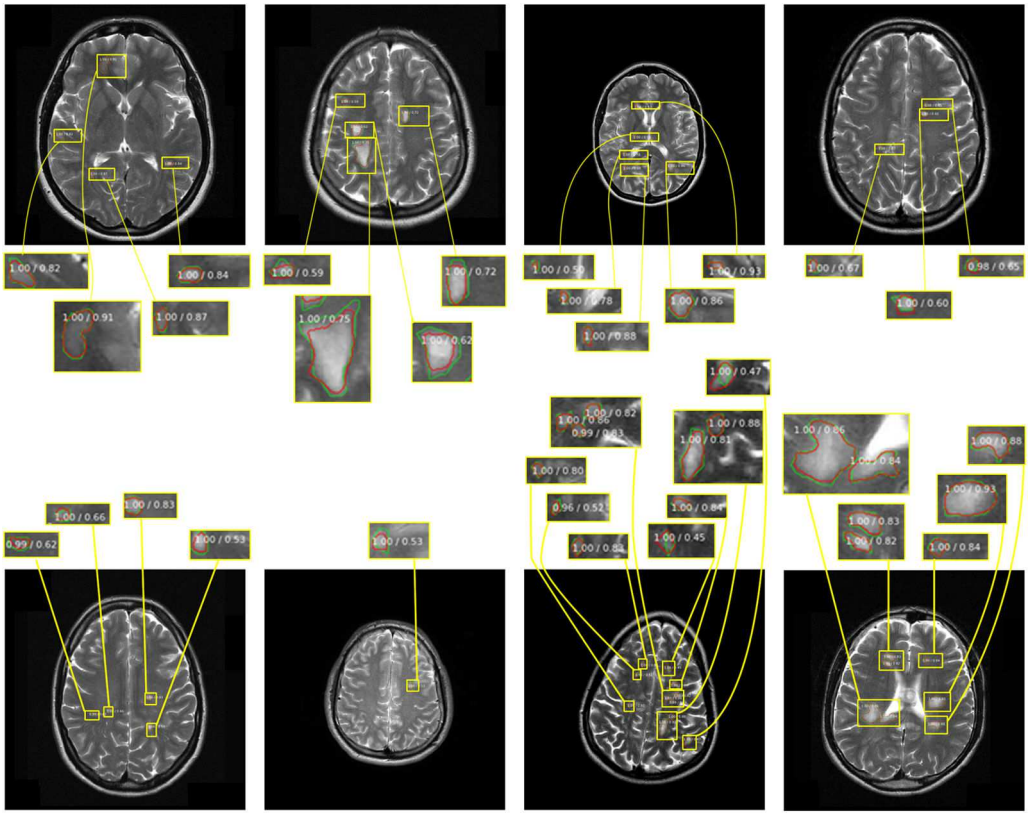

Fig. 13 *Comparison of MS lesions detected by the model proposed on MR images and MS lesions determined by the expert*

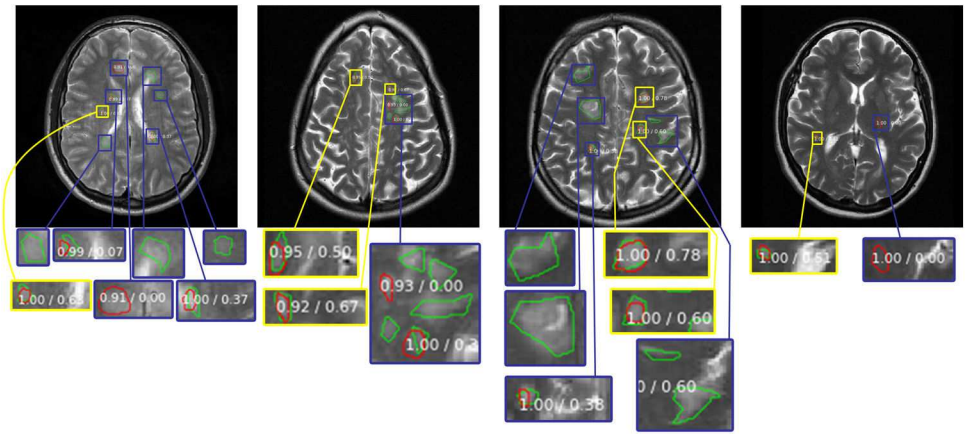

Fig. 14 *Some MS lesions detected incorrectly on MR images in the proposed study*

segmentation of MS lesions using U-Net algorithm are denoted on the eHealth dataset, on the same original MR images and the ground truths marked by the expert shown in Fig. 13. In the experimental studies conducted for the U-Net algorithm, the same training and test sets in the Mask R-CNN model were used. In these experimental studies on the MC-R101 backbone, the number of epoch was determined as 100 and data augmentation process was applied. In detection of MS lesions using U-Net algorithm, the average performance scores such as 78.76%±9.25 DC, 9.21%±4.63 VOE were obtained on 86 MR images in the test set created for the eHealth dataset.

A visual comparison of the method proposed in our study on another public dataset, UMCL MS dataset, was denoted in Fig. 16. It can be seen from the visual results presented on some FLAIR images in the dataset that the proposed Mask R-CNN method (Fig. 16*c*) is more successful than the segmentation results with U-Net (Fig. 16*d*). In the experimental studies on the UMCL dataset, 502 training and 98 test set images with different numbers of MS lesions were selected to be similar to the sets in the other dataset. In the test processes carried out with the same parameters applied for the eHealth dataset, an average of 81.86%±9.74 DC similarity value and 70.88%±7.32 LTPR value were achieved for the proposed Mask R-CNN method on UMCL dataset, while only 72.21%±6.58 DC value and 64.56%±5.47 LTPR value were obtained with the U-Net method.

In our study, the effect of noise in MR images on the performance of the obtained results was also investigated in detecting MS lesions. For this, firstly, Gaussian noises at a rate of 0.1 were added to the MR images in the test and training sets created from the eHealth dataset. Afterwards, detection of MS lesions in MR images was performed using the proposed Mask R-CNN model. The average 71.38% DC and 25.53% VOE values were obtained in the MR images of the test set with Gaussian noise. Then, the noise in the MR images was removed using the spatially adaptive image denoising method, proposed by Huang *et al.* [69, 70]. It is seen that MS lesions were detected more successfully using the proposed Mask R-CNN method after the Gaussian noise was removed. In the experimental studies performed using MR images in the denoising test set, 77.66%6.41± DC and 17.39%±5.87 VOE measurement results were obtained using the proposed Mask R-CNN method. Although these results show that removing noise from MR images improves detection

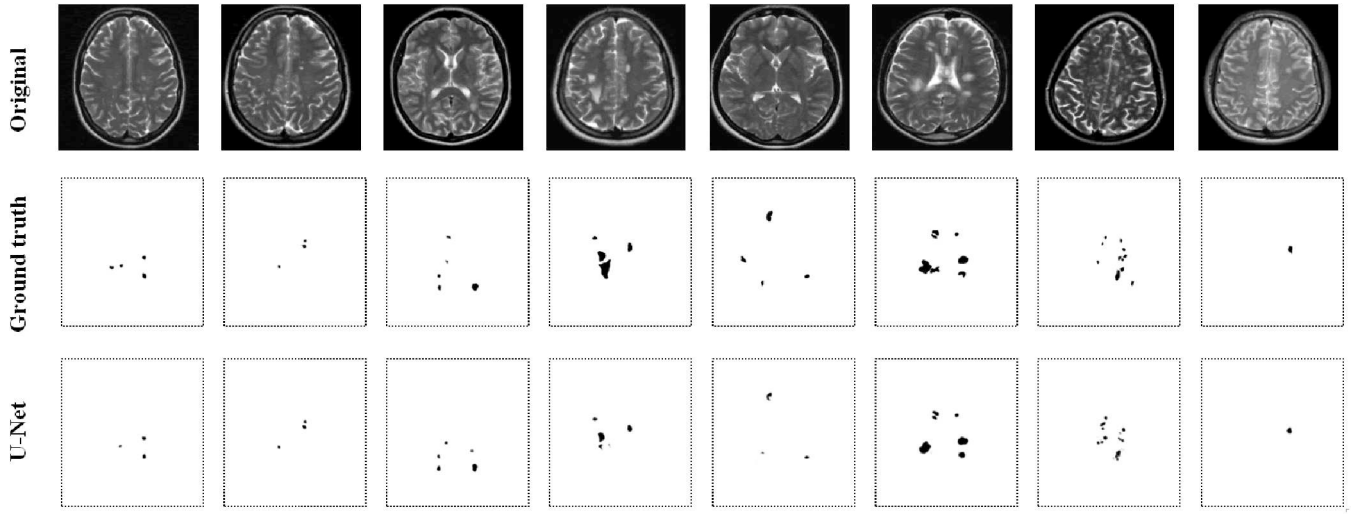

Fig. 15 *MS lesion detection using U-Net on eHealth dataset*

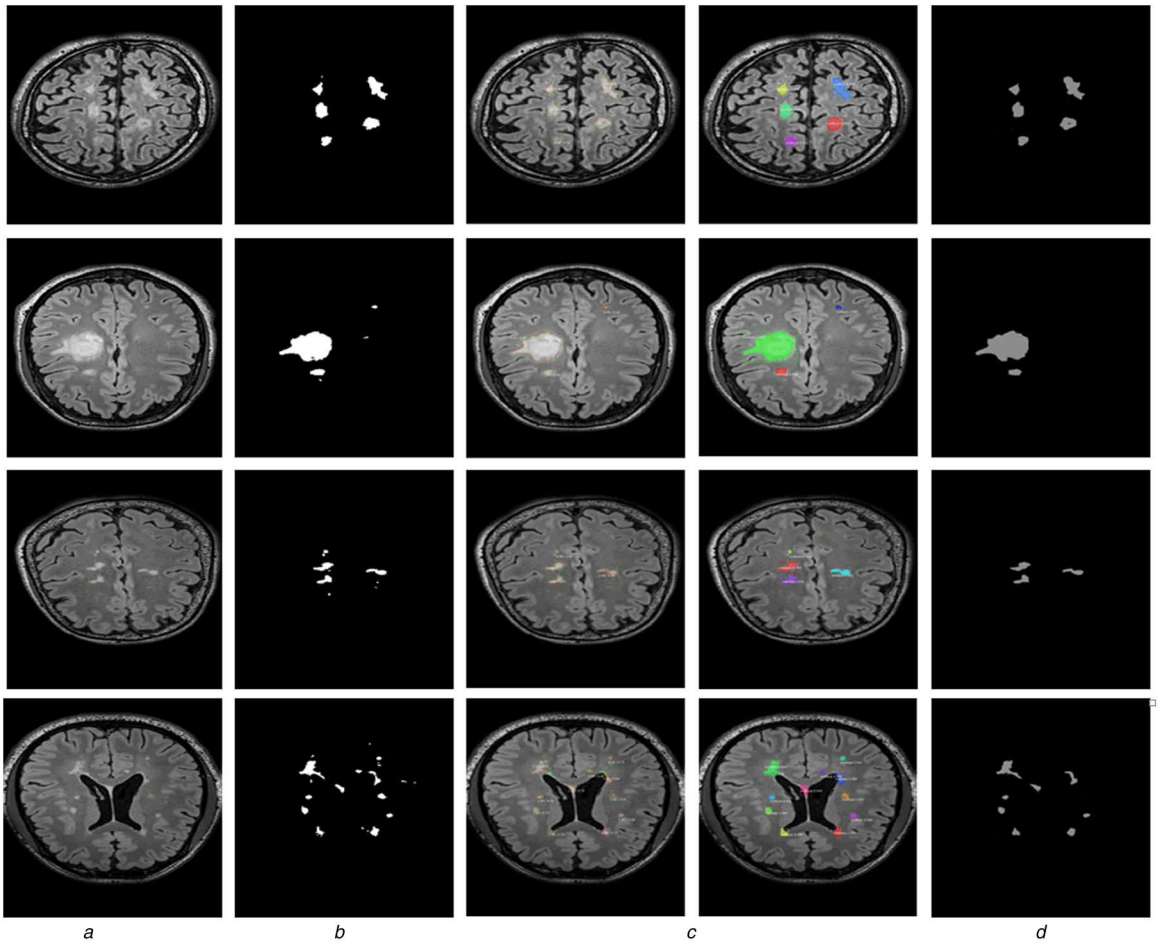

Fig. 16 *Visual comparison of segmentation results of MS lesions in MR images via the proposed Mask R-CNN and U-Net methods on UMCL MS dataset*
(a) Original MR image, ***(b)*** Ground truth, ***(c)*** Segmentation via the proposed Mask R-CNN, ***(d)*** Segmentation via U-Net

performance of MS lesions, they are still far from the results obtained with the original noiseless MR images.

It is very difficult to compare the previous studies on the computer aided detection of MS lesions on MR images due to the lack of the same data, different detection algorithms, and using different similarity metrics. However, the comparison of the results of this study with some of the previously proposed studies according to the DC similarity coefficient and LTPR rate are given in Table 10. As can be seen from this table, it can be concluded that the results of this study are noteworthy considering the presence of lesions, which are quite small in dataset.

6 Conclusion

The contribution of computer-aided tools to assist physicians in diagnosing and follow-up MS on MR images has gained remarkable progress in the field in recent years. The lesion detection by manual selection by physicians consists of subjective and time-consuming procedural sequences. For this reason, automatic detection of MS lesions using MR images is of great importance in terms of both time consuming and cost. In this study, a Mask R-CNN based state-of-art method, which can be used as a secondary tool in the decision-making process of physicians, was proposed for the detection of MS lesions on MR images. In experimental studies conducted on a two public datasets, the

Table 10 Comparison of the results of this study with the results of previous studies

Study	Dataset	Method	DC, %	LTPR, %
Brosch *et al.* [46]	MICCAI 2008, ISBI 2015	deep 3D convolutional encoder networks	*NA*, 68.4	51.6, 78.3
Valverde *et al.* [37]	MICCAI 2008	cascaded 3D CNN	56.0	*NA*
Birenbaum *and* Greenspan [44]	ISBI 2015	multi-view CNN	62.70	*NA*
Ravnik *et al.* [38]	UMCL	CNN	81.49	69.95
Zhao *et al.* [10]	MICCAI 2008,	a level set method	55.0	*NA*
Atlason *et al.* [45]	the AGES-Reykjavik, MICCAI 2017	CNN autoencoder	77.0, 67.0	64.0, 40.0
Wang *et al.* [30]	MICCAI 2008	adaptive sparse Bayesian model	42.0	*NA*
Gessert *et al.* [49]	their own datasets	two-path CNNs	65.6, 65.2	73.1, 79.4
Proposed study	eHealth, UMCL	Mask R-CNN with proposed ROI detection	84.90,81.86	73.75, 70.88

proposed method detected successfully MS lesions on MR images, including small ones. In addition, many previously proposed studies on MS lesion detection were evaluated and a short survey study was conducted on the previous studies.

The contributions of this study can be summarised as follows. (i) In this study, which was proposed for the detection of MS lesions on MR images, performance comparison was conducted on the ResNet50 and ResNet101 backbones. As a result of experimental studies, Dice similarity was achieved as 84.9% by using the MC-R101 Mask R-CNN model modified using ResNet101. (ii) We improved the ROI detection stage with RPN in the Mask R-CNN for adaptation in different lesion sizes. (iii) A computer-aided decision support system to assist physicians for the detection of small lesions such as MS is presented as a secondary tool. (iv) Speed performance tests were also conducted for the proposed MC-R50 and MC-R101 Mask R-CNN models for single GPU and double GPU hardware structures. With the performance tests, the most efficient operating structure for the double GPU was determined and the results have been revealed. (v) As a dataset in follow-up structure where MS patients can be followed up periodically was used within the scope of the study, a method that allows decision making by evaluating MR images of different people at different times was developed. (vi) In the study, the change of the operating speed according to the iteration number, number of GPUs and the number of IPG of Mask R-CNN architecture was evaluated. It was figured out that the structure operates with relation to BS calculated from the combination of these values. In calculating the optimum point for the efficiency of the study, it was showed that the processing time per image decreases as the BS increases.

In the following studies, it is planned to create a dataset from MR images obtained from different resolutions, sizes and scanners for achieving high detection performance. In addition, tests in different configurations can be performed on a standard dataset to achieve results on multi GPU and GPU performance. Moreover, further studies can focus on increasing the detection performance of MS lesions with a new model without limitations of the Mask R-CNN model. Besides, it is planned to conduct periodic studies on MS follow-up on dataset.

7 Acknowledgments

The authors of this study thank Scientific Research Projects Department of Bilecik Seyh Edebali University for providing the used workstation within project number 2019–01.BŞEÜ.25–02. They also thank the eHealth Laboratory and UMCL, which brought the used MS datasets to the scientific world.

8 References

[1] Mortazavi, D., Kouzani, A.Z., Soltanian-Zadeh, H.: 'Segmentation of multiple sclerosis lesions in Mr images: a review', *Neuroradiology*, 2012, **54**, (4), pp. 299–320

[2] Calabresi, P.A.: 'Diagnosis and management of multiple sclerosis', *Am. Fam. Physician*, 2004, **70**, (10), pp. 1935–1944

[3] Gooch, C.L., Pracht, E., Borenstein, A.R.: 'The burden of neurological disease in the United States: a summary report and call to action', *Ann. Neurol.*, 2017, **81**, (4), pp. 479–484

[4] Almasi-Hashiani, A., Sahraian, M.A., Eskandarieh, S.: 'Evidence of an increased prevalence of multiple sclerosis: a population-based study of Tehran registry during 1999–2018', *BMC Neurol.*, 2020, **20**, pp. 1–7

[5] King, R.: *The Multiple Sclerosis International Federation*, (Atlas of MS, September 2020), 3rd Edn, https://www.atlasofms.org/map/global/epidemiology/number-of-people-with-ms (Accessed: 08 June2020)

[6] Wallin, M.T., Culpepper, W.J., Nichols, E., *et al.*: 'Global, regional, and national burden of multiple sclerosis 1990–2016: a systematic analysis for the global burden of disease study 2016', *Lancet Neurol.*, 2019, **18**, (3), pp. 269–285

[7] Multiple Sclerosis: Facts, Statistics, and You, https://www.healthline.com/health/multiple-sclerosis/facts-statistics-infographic, (Accessed: 08 June 2020)

[8] Goldenberg, M.M.: 'Multiple sclerosis review', *Pharmacy Therapeutics*, 2012, **37**, (3), pp. 175–184

[9] McDonald, W.I., Compston, A., Edan, G., *et al.*: 'Recommended diagnostic criteria for multiple sclerosis: guidelines from the international panel on the diagnosis of multiple sclerosis', *Ann. Neurology, Off. J. Am. Neurol. Assoc. Child Neurol. Soc.*, 2001, **50**, (1), pp. 121–127

[10] Zhao, Y., Guo, S., Luo, M., *et al.*: 'A level set method for multiple sclerosis lesion segmentation', *Magn. Reson. Imaging*, 2018, **49**, pp. 94–100

[11] Solomon, A.J., Naismith, R.T., Cross, A.H.: 'Misdiagnosis of multiple sclerosis: impact of the 2017 Mcdonald criteria on clinical practice', *Neurology*, 2019, **92**, (1), pp. 26–33

[12] Bosc, M., Heitz, F., Armspach, J.-P., *et al.*: 'Automatic change detection in multimodal serial mri: application to multiple sclerosis lesion evolution', *NeuroImage*, 2003, **20**, (2), pp. 643–656

[13] Meller, J., Strutz, F., Siefker, U., *et al.*: 'Early diagnosis and follow-up of aortitis with [18 F] fdg pet and mri', *Eur. J. Nucl. Med. Mol. ImAging*, 2003, **30**, (5), pp. 730–736

[14] Laakso, M.P., Lehtovirta, M., Partanen, K., *et al.*: 'Hippocampus in alzheimer's disease: A 3-year follow-up mri study', *Biol. Psychiatry*, 2000, **47**, (6), pp. 557–561

[15] Traboulsee, A., Simon, J., Stone, L., *et al.*: 'Revised recommendations of the consortium of Ms centers task force for a standardized mri protocol and clinical guidelines for the diagnosis and follow-up of multiple sclerosis', *Am. J. Neuroradiology*, 2016, **37**, (3), pp. 394–401

[16] Lana-Peixoto, M.A., Pedrosa, D., Talim, N., *et al.*: 'Neuromyelitis optica spectrum disorder associated with dengue virus infection', *J. Neuroimmunol.*, 2018, **318**, pp. 53–55

[17] Deguchi, I., Tanahashi, N., Takao, M.: 'Clinical study of intravenous, low-dose recombinant tissue plasminogen activator for acute cerebral infarction: comparison of treatment within 3 hours versus 3-4.5 hours', *J. Stroke Cerebrovasc. Dis.*, 2018, **27**, (4), pp. 1033–1040

[18] Desse, N., Sellier, A., Bernard, C., *et al.*: 'Fatal acute disseminated encephalomyelitis (adem) after third ventricle colloid cyst resection with ultrasonic aspirator during neuroendoscopic procedure', *Acta Neurochir.*, 2018, **160**, (9), pp. 1789–1792

[19] Shrivastava, N., Bharti, J.: 'Breast tumor detection and classification based on density', *Multimedia Tools Appl.*, 2020, **79**, (35), pp. 26467–26487

[20] Gros, C., De Leener, B., Badji, A., *et al.*: 'Automatic segmentation of the spinal cord and intramedullary multiple sclerosis lesions with convolutional neural networks', *Neuroimage*, 2019, **184**, pp. 901–915

[21] Shrivastava, N., Bharti, J.: 'A comparative analysis of medical image segmentation'. Int. Conf. on Advanced Computing Networking and Informatics, Indore, India, 2019, pp. 459–467

[22] Bakshi, R.: 'Fatigue associated with multiple sclerosis: diagnosis, impact and management', *Multiple Sclerosis J.*, 2003, **9**, (3), pp. 219–227

[23] Miller, D., Weinshenker, B.G., Filippi, M., *et al.*: 'Differential diagnosis of suspected multiple sclerosis: a consensus approach', *Multiple Sclerosis J.*, 2008, **14**, (9), pp. 1157–1174

[24] Poser, C.M., Paty, D.W., Scheinberg, L., *et al.*: 'New diagnostic criteria for multiple sclerosis: guidelines for research protocols', *Ann. Neurol., Off. J. Am. Neurol. Assoc. Child Neurol. Soc.*, 1983, **13**, (3), pp. 227–231

[25] Miller, D., Barkhof, F., Montalban, X., *et al.*: 'Clinically isolated syndromes suggestive of multiple sclerosis, part i: natural history, pathogenesis, diagnosis, and prognosis', *Lancet Neurol.*, 2005, **4**, (5), pp. 281–288

[26] Danelakis, A., Theoharis, T., Verganelakis, D.A.: 'Survey of automated multiple sclerosis lesion segmentation techniques on magnetic resonance imaging', *Comput. Med. Imaging Graph.*, 2018, **70**, pp. 83–100

[27] Yamamoto, D., Arimura, H., Kakeda, S., *et al.*: 'Computer-aided detection of multiple sclerosis lesions in brain magnetic resonance images: false positive reduction scheme consisted of rule-based, level set method, and support vector machine', *Comput. Med. Imaging Graph.*, 2010, **34**, (5), pp. 404–413

[28] Solari, A., Motta, A., Mendozzi, L., *et al.*: 'Computer-aided retraining of memory and attention in people with multiple sclerosis: a randomized, double-blind controlled trial', *J. Neurol. Sci.*, 2004, **222**, (1–2), pp. 99–104

[29] Ghahazi, M.A., Zarandi, M.F., Harirchian, M., *et al.*: 'Fuzzy rule based expert system for diagnosis of multiple sclerosis'. 2014 IEEE Conf. on Norbert Wiener in the 21st Century (21CW), Boston, MA, USA, 2014, pp. 1–5

[30] Wang, J., Liu, M., Zhang, C., *et al.*: 'An adaptive sparse Bayesian model combined with probabilistic label fusion for multiple sclerosis lesion segmentation in brain mri', *Future Gener. Comput. Syst.*, 2020, **105**, pp. 695–704

[31] Souplet, J.-C., Lebrun, C., Ayache, N., *et al.*: 'An automatic segmentation of T2-flair multiple sclerosis lesions'. MICCAI-Multiple Sclerosis Lesion Segmentation Challenge Workshop, New York, NY, USA, United States, 2008, pp. 1–11

[32] Schmidt, P., Gaser, C., Arsic, M., *et al.*: 'An automated tool for detection of flair-hyperintense white-matter lesions in multiple sclerosis', *Neuroimage*, 2012, **59**, (4), pp. 3774–3783

[33] Roura, E., Oliver, A., Cabezas, M., *et al.*: 'A toolbox for multiple sclerosis lesion segmentation', *Neuroradiology*, 2015, **57**, (10), pp. 1031–1043

[34] Zhang, Y., Lu, S., Zhou, X., *et al.*: 'Comparison of machine learning methods for stationary wavelet entropy-based multiple sclerosis detection: decision tree, K-nearest neighbors, and support vector machine', *Simulation*, 2016, **92**, (9), pp. 861–871

[35] Wu, X., Lopez, M.: 'Multiple sclerosis slice identification by haar wavelet transform and logistic regression'. Advances in Materials, Machinery, Electrical Engineering (AMMEE 2017), Tianjin, People's Republic of China, 2017, pp. 50–55

[36] Brosch, T., Yoo, Y., Tang, L.Y., *et al.*: 'Deep convolutional encoder networks for multiple sclerosis lesion segmentation'. Int. Conf. on Medical Image Computing and Computer-Assisted Intervention, Munich, Germany, 2015, pp. 3–11

[37] Valverde, S., Cabezas, M., Roura, E., *et al.*: 'Improving automated multiple sclerosis lesion segmentation with a cascaded 3d convolutional neural network approach', *NeuroImage*, 2017, **155**, pp. 159–168

[38] Ravnik, D., Jerman, T., Pernuš, F., *et al.*: 'Dataset variability leverages white-matter lesion segmentation performance with convolutional neural network'. Medical Imaging 2018: Image Processing, Houston, TX, United States, 2018, p. 105741J

[39] Cerasa, A., Bilotta, E., Augimeri, A., *et al.*: 'A cellular neural network methodology for the automated segmentation of multiple sclerosis lesions', *J. Neurosci. Methods*, 2012, **203**, (1), pp. 193–199

[40] Zhang, Y.-D., Pan, C., Sun, J., *et al.*: 'Multiple sclerosis identification by convolutional neural network with dropout and parametric relu', *J. Comput. Sci.*, 2018, **28**, pp. 1–10

[41] Maleki, M., Teshnehlab, M., Nabavi, M.: 'Diagnosis of multiple sclerosis (Ms) using convolutional neural network (cnn) from mris', *Glob. J. Med. Plant Res.*, 2012, **1**, (1), pp. 50–54

[42] Wang, S.-H., Tang, C., Sun, J., *et al.*: 'Multiple sclerosis identification by 14-layer convolutional neural network with batch normalization, dropout, and stochastic pooling', *Front. Neurosci.*, 2018, **12**, pp. 1–11

[43] Nair, T., Precup, D., Arnold, D.L., *et al.*: 'Exploring uncertainty measures in deep networks for multiple sclerosis lesion detection and segmentation', *Med. Image Anal.*, 2020, **59**, p. 101557

[44] Birenbaum, A., Greenspan, H.: 'Multi-view longitudinal cnn for multiple sclerosis lesion segmentation', *Eng. Appl. Artif. Intell.*, 2017, **65**, pp. 111–118

[45] Atlason, H.E., Love, A., Sigurdsson, S., *et al.*: 'Segae: unsupervised white matter lesion segmentation from brain mris using a cnn autoencoder', *NeuroImage, Clin.*, 2019, **24**, p. 102085

[46] Brosch, T., Tang, L.Y., Yoo, Y., *et al.*: 'Deep 3d convolutional encoder networks with shortcuts for multiscale feature integration applied to multiple sclerosis lesion segmentation', *IEEE Trans. Med. Imaging*, 2016, **35**, (5), pp. 1229–1239

[47] Valcarcel, A.M., Linn, K.A., Vandekar, S.N., *et al.*: 'Mimosa: an automated method for intermodal segmentation analysis of multiple sclerosis brain lesions', *J. Neuroimaging*, 2018, **28**, (4), pp. 389–398

[48] Gabr, R.E., Coronado, I., Robinson, M., *et al.*: 'Brain and lesion segmentation in multiple sclerosis using fully convolutional neural networks: a large-scale study', *Multiple Sclerosis J.*, 2020, **26**, (10), pp. 1217–1226

[49] Gessert, N., Krüger, J., Opfer, R., *et al.*: 'Multiple sclerosis lesion activity segmentation with attention-guided two-path cnns', *Comput. Med. Imaging Graph.*, 2020, **84**, p. 101772

[50] Loizou, C.P.: eHealth Lab, MRI Lesion Segmentation in Multiple Sclerosis Database, http://ehealthlab.cs.ucy.ac.cy/old/doc/Publications/Datasets/80carotid%20plaques%20-%20Free%20Dataset.zip, (Accessed: 08 June2020)

[51] Loizou, C.P., Murray, V., Pattichis, M.S., *et al.*: 'Multiscale amplitude-modulation frequency-modulation (Am–Fm) texture analysis of multiple sclerosis in brain mri images', *IEEE Trans. Inf. Technol. Biomed.*, 2010, **15**, (1), pp. 119–129

[52] Loizou, C.P., Kyriacou, E.C., Seimenis, I., *et al.*: 'Brain white matter lesion classification in multiple sclerosis subjects for the prognosis of future disability', *Intell. Decis. Technol.*, 2013, **7**, (1), pp. 3–10

[53] Loizou, C.P., Pantziaris, M., Seimenis, I., *et al.*: 'Brain Mr image normalization in texture analysis of multiple sclerosis'. 2009 9th Int. Conf. on Information Technology and Applications in Biomedicine, Larnaca, Cyprus, 2009, pp. 1–5

[54] Loizou, C.P., Petroudi, S., Seimenis, I., *et al.*: 'Quantitative texture analysis of brain white matter lesions derived from T2-weighted Mr images in Ms patients with clinically isolated syndrome', *J. Neuroradiol.*, 2015, **42**, (2), pp. 99–114

[55] Lesjak, Ž., Galimzianova, A., Koren, A., *et al.*: 'A novel public Mr image dataset of multiple sclerosis patients with lesion segmentations based on multi-rater consensus', *Neuroinformatics*, 2018, **16**, (1), pp. 51–63

[56] Ucml Laboratory of Imaging Technologies 3d Mr Image Database of Multiple Sclerosis Patients with White Matter Lesion Segmentations, http://lit.fe.uni-lj.si/tools.php?lang=eng, (Accessed: 20 October 2020)

[57] Krizhevsky, A., Sutskever, I., Hinton, G.E.: 'Imagenet classification with deep convolutional neural networks'. Advances in Neural Information Processing Systems, Lake Tahoe, NV, USA, 2012, pp. 1097–1105

[58] Özkan, İ., Ülker, E.: 'Derin Öğrenme Ve görüntü analizinde kullanılan derin Öğrenme modelleri', *Gaziosmanpaşa Bilimsel Araştırma Dergisi*, 2017, **6**, (3), pp. 85–104

[59] Girshick, R., Donahue, J., Darrell, T., *et al.*: 'Rich feature hierarchies for accurate object detection and semantic segmentation'. Proc. of the IEEE Conf. On Computer Vision And Pattern Recognition, Columbus, OH, 2014, pp. 580–587

[60] He, K., Gkioxari, G., Dollár, P., *et al.*: 'Mask R-cnn'. Proc. of the IEEE Int. Conf. On Computer Vision, Venice, Italy, 2017, pp. 2961–2969

[61] Wu, M., Yue, H., Wang, J., *et al.*: 'Object detection based on rgc mask R-cnn', *IET Image Process.*, 2020, **14**, (8), pp. 1502–1508

[62] Xu, B., Wang, W., Falzon, G., *et al.*: 'Automated cattle counting using mask R-cnn in quadcopter vision system', *Comput. Electron. Agric.*, 2020, **171**, p. 105300

[63] Abdulla, W.: 'Mask R-Cnn for Object Detection and Instance Segmentation on Keras and Tensorflow: Matterport/Mask_Rcnn', Python, Matterport, Inc, Available at https://github.com/matterport, 2018

[64] Bui, N.L., Ong, S.H., Foong, K.W.C.: 'Automatic segmentation of the nasal cavity and paranasal sinuses from cone-beam Ct images', *Int. J. Comput. Assist. Radiol. Surg.*, 2015, **10**, (8), pp. 1269–1277

[65] Aslani, S., Dayan, M., Storelli, L., *et al.*: 'Multi-branch convolutional neural network for multiple sclerosis lesion segmentation', *NeuroImage*, 2019, **196**, pp. 1–15

[66] Ronneberger, O., Fischer, P., Brox, T.: 'U-Net: convolutional networks for biomedical image segmentation'. Int. Conf. on Medical image computing and computer-assisted intervention, Munich, Germany, 2015, pp. 234–241

[67] Jeevakala, S., Sreelakshmi, C., Ram, K., *et al.*: 'Artificial intelligence in detection and segmentation of internal auditory canal and its nerves using deep learning techniques', *Int. J. Comput. Assist. Radiol. Surg.*, 2020, **15**, pp. 1859–1867

[68] Hu, X., Yang, H.: 'Dru-net: a novel u-net for biomedical image segmentation', *IET Image Process.*, 2019, **14**, (1), pp. 192–200

[69] Huang, Z., Zhang, Y., Li, Q., *et al.*: 'Spatially adaptive denoising for X-ray cardiovascular angiogram images', *Biomed. Signal Proc. Control*, 2018, **40**, pp. 131–139

[70] Huang, Z., Li, Q., Zhang, T., *et al.*: 'Iterative weighted sparse representation for X-ray cardiovascular angiogram image denoising over learned dictionary', *IET Image Process.*, 2017, **12**, (2), pp. 254–261